ACADEMIA ROMÂNĂ
Revue Roumaine de Chimie
http://web.icf.ro/rrch/

Rev. Roum. Chim.,
2021, *66*(12), 895–906
DOI: 10.33224/rrch.2021.66.12.02

Papers

A RAPID AND SENSITIVE METHOD FOR SEPARATION/PRECONCENTRATION AND DETERMINATION OF CU $^{2+}$ FROM AQUEOUS SOLUTION USING MODIFIED MAGNETIC GRAPHENE OXIDE NANOCOMPOSITE

Rosa KALANTARI, Ali MOGHIMI* and Fariborz AZIZINEZHAD

Department of Chemistry, Varamin-Pishva Branch, Islamic Azad University, Varamin, Iran

Received January 23, 2021

In this research, magnetic graphene oxide composite functionalized with chitosan (mGO-CS) was utilized to extract, preconcentrate, and determine the trace amount of Cu^{2+} ions in aqueous samples. The Flame Atomic Absorption Spectrometry (FAAS) method determined Cu^{2+} ions concentration in aqueous solutions. FTIR, XRD, TGA,VSM, and SEM techniques were performed to characterize the synthesized composite's chemical structure, surface morphology, and magnetic properties. The parameters effective on the extraction efficiency were evaluated and optimized. In optimum situations, the linearity limit for the determination of Cu^{2+} ions was about 0.03–8.00 μg mL^{-1}. LOQ and LOD values were obtained 0.03μg mL^{-1} and 0.01μg mL^{-1}, respectively. The repeatability coefficient of the suggested method was 2.16% (RSD%). Finally, it was found that the proposed method represents a novel technique with advantages such as the higher precision and efficiency, economical and cost-effective process, and the ability of fast and straightforward separation with the lower detection limit.

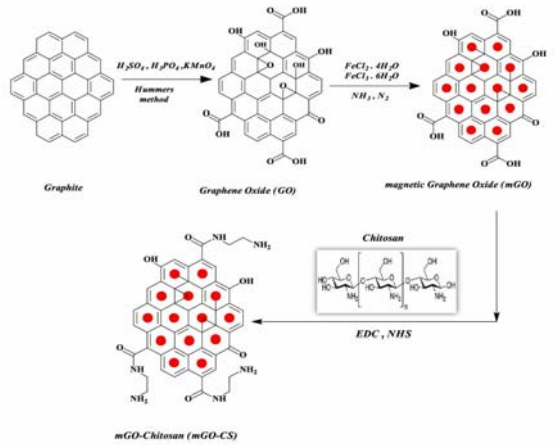

INTRODUCTION

Releasing heavy metals into the environment due to their toxicity is a threat to living organisms' health. Hence, it is necessary to remove these pollutants from the environment.[1] The excess amount of Cu^{2+} ions in drinking water and the other food cause various disease in humans. Intaking too much copper causes anemia and iron deficiency by interfering with the absorption of iron and zinc.[2] The adsorption technique is one of the standard methods for removing heavy metals and drug adsorption from water sources. Considering the various advantages of this technique, including simplicity, straightforward performance, lower cost, and higher efficiency, it has recently received much attention.[3] Magnetic nanoparticles are extensively used to remove heavy metals from wastewater. Due to the high surface-to-volume ratio, magnetic nanoparticles increases adsorption capacity increases. Moreover, their surface can be modified with other materials. They are also non-toxic and biocompatible. They can be separated from the solution and recovered because of their magnetic properties.[4-5] The solid-phase extraction technique, which is based on magnetic adsorbents, is called magnetic solid-phase extraction (MSPE). The MSPE technique can

* Corresponding author: kamran9537@yahoo.com; alimoghimi@iauvaramin.ac.ir

separate small amounts of the target analyte from a large sample volume without further centrifugation, filtration, and expensive equipment. The other advantage of this method is the higher efficiency and the lower solvent consumption.[6] Graphene oxide can be used as an adsorbent to remove heavy metals in water treatment. The presence of hydroxyl, epoxy and carboxyl functional groups in graphene oxide facilitates the creation of the metal-organic coordination system. Graphene oxide has many excellent properties such as the large cross-section, the great thermal and chemical stability, the high porosity, and advanced adsorption capacity. The high cross-sectional area causes the high adsorption capacity. To increase the efficiency of graphene oxide as an adsorbent, its surface is chemically or physically functionalized and modified before use.[7-8] Chitosan is a natural amino polysaccharide obtained from the deacetylation of chitin under alkaline conditions. It has excellent and attractive characteristics, including non-toxicity, high adsorption properties, degradability in nature, biocompatibility, environmentally friendly, cost-effectiveness, and the ability to remove heavy metals. The negative charge of amino groups on the surface of chitosan facilitates the adsorption of biomolecules and heavy metals.[2,9] In this study, magnetic graphene oxide composite (mGO-CS), as the adsorbent of Cu^{2+} ions from aqueous samples, was characterized and synthesized by Vibrating Sample Magnetometer (VSM), Fourier Transform Infrared Spectra (FTIR), X-ray Diffraction (XRD), Thermogravimetric Analysis (TGA), and Scanning Electron Microscope (SEM) techniques. Then, the influential and essential parameters in Cu^{2+} ions extraction such as pH, the extent of adsorbent, the extraction time, the kind and content of eluent, and the sample volume were investigated and optimized. The Equilibrium adsorption data, kinetic studies of the adsorption procedure and thermodynamic parameters were analyzed. Finally, the usability of the proposed method to remove Cu^{2+} ions in various aqueous samples was investigated.

EXPERIMENTAL

1. Materials

Chitosan with 80 mesh, 96% degree of deacetylation, and average-molecular weight of 6.34×10^5, Graphite flake (7-10 micron), $FeCl_3{\cdot}6H_2O$, and $FeCl_2{\cdot}4H_2O$ were bought from Sigma Aldrich. The reagents N-hydroxyl Succinimide (NHS) and 1-ethyl-3-(3-dimethyl aminopropyl) carbodiimide hydro-chloride (EDC) were taken from Aldrich products. Stock solutions (1000 mg L^{-1}) of Cu^{2+} got ready to dissolve the proper amount of its corresponding nitrate salts (Merck, Darmstadt, Germany). All the other reagents were of analytical grade with the highest purity, and the deionized water was utilized to prepare all the solutions.

2. Apparatus

The ions mentioned above were measured using an Agilent Series AA (model 240 AA) flame atomic absorption spectrometer (USA) with hollow cathode copper lamps and an air-acetylene flame. The pH was determined to employ the Metrohm692 pH meter (Herisau, Switzerland). The FTIR spectrum was obtained using an FT-IR spectrometer (Perkin Elmer, USA) in the spectral range of 4000-400 cm^{-1} through the standard KBr disk technique. A Philips-PW 12C diffractometer (Philips PW, Amsterdam, Netherlands) was utilized to collect the powder XRD pattern through Cu Kα radiation. The Scanning Electron Microscopy (SEM) image was achieved with a scanning electron microscope (TESCAN Vega 3 model). Bahr STA-503 (Germany) was employed to carry out a thermogravimetric analysis (TGA). The magnetization evaluations were carried out on an AGFM/VSM3886 VSM (Meghnatis Daghigh Kavir Co., Iran). An Nd-Fe-B strong magnet (15 cm × 12 cm × 5 cm, 1.4 T) was employed for magnetic separation. We used an Ultrasonic bath (Sonorex digitec, DT255H, Germany) and an oven (Universal model UF 55, Germany) for the magnetic graphene oxide nano-composite preparation and digestion steps.

3. Synthesis of graphene oxide sheets (GO)

The synthesis of GO was performed utilizing a modified Hummers technique by the oxidation of graphite powder.[10] Concentrated H_3PO_4 (100 mL) and H_2SO_4 (70 mL) were added to 3 g of graphite powder. The reaction was performed in an ice bath for 30 min. Under continuous stirring, the mixture was further oxidized with 9 g of $KMnO_4$ in an ice bath, and the temperature of the reactant was maintained at 4ºC for one h. The mix was then blended at 50ºC in a water bath for 24 h to allow complete oxidation of the graphite. Afterward, 150 mL of water was slowly added to the mixture with an ice bath. A great extent of heat was discharged in this reaction. The solution was further diluted with 100 mL deionized water and 35 mL of 30% H_2O_2. Ultimately, the mix was centrifuged and washed with 15% HCl and deionized water. The pH was regulated to 7. The final sample was dried at 50ºC for 24 h in an oven.

4. Synthesis of magnetic graphene oxide (mGO)

About 0.3 g of synthesized GO was primarily scattered in 25 mL of deionized water (maintained for two h in an ultrasonic irradiation bath). Subsequently, 1.081g ferric chloride ($FeCl_3{\cdot}6H_2O$, 2 mmol) and 0.397g Ferrous chloride ($FeCl_2{\cdot}4H_2O$, 4 mmol) were solved in 25 mL of deionized water. Afterward, this blend was added to the GO dilution under blending and placed in a 60ºC hot water bath for about 30 min. After cooling, the black mixture of 170 mL of 1.25 mol L^{-1} NH_3 dilution was added dropwise into the mix and then maintained under continuous mixing at 60°C for 3 h. During this procedure, the nitrogen gas was continuously blown into the solution to stop the entry of oxygen. After the solution cooled down, it was washed four times with deionized water, and the sediment was separated from the solution using a 1.4 Tesla magnet. The final residue was dried out completely in a vacuum oven at 50ºC for 5 h.[11]

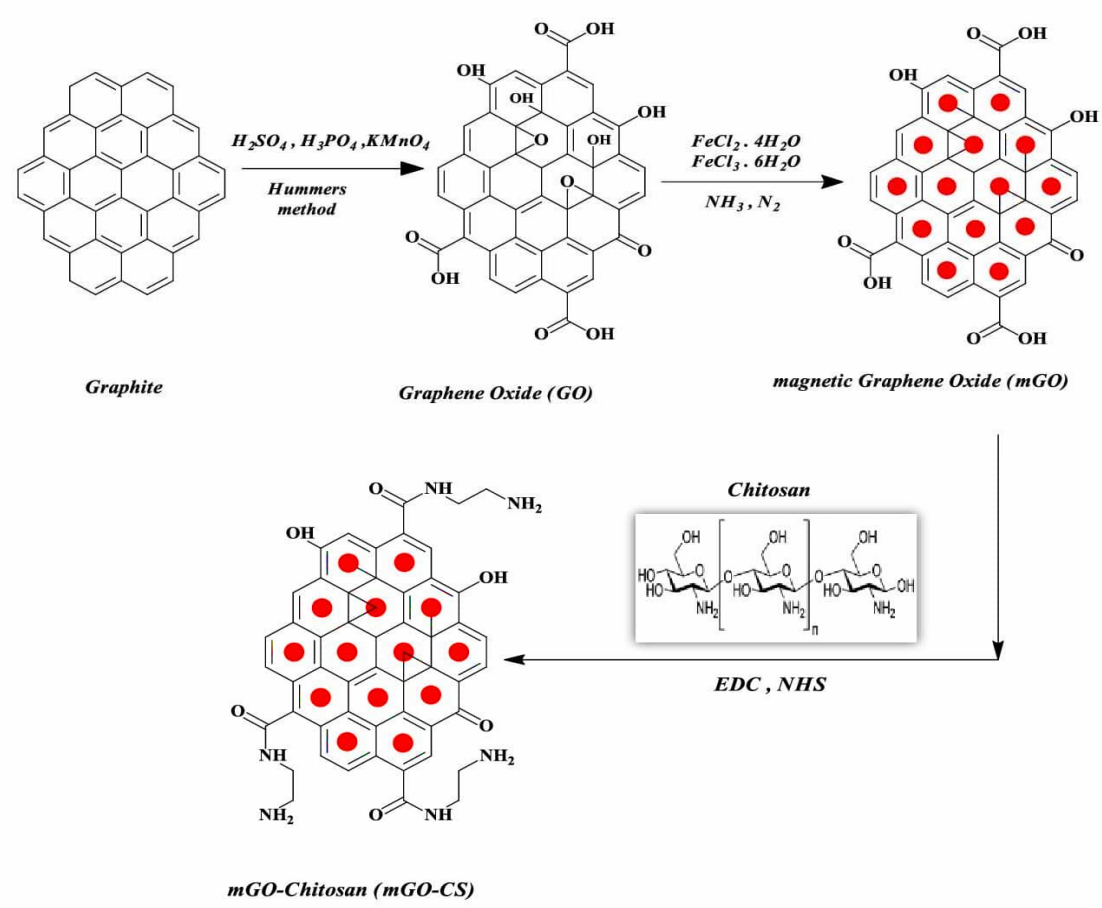

Fig. 1 – Scheme of mGO-CS synthesis steps.

5. Synthesis of magnetic graphene oxide-chitosan nanocomposite (mGO-CS)

At this point, 0.1 g of the magnetic Graphene Oxide (mGO) was ultrasonically dispersed in 50 mL of deionized water. 1 mL of 0.05 mol L^{-1} N-(3-dimethyl aminopropyl)-N′-ethyl carbodiimide (EDC) solution and 1 mL of 0.05 mol L^{-1} N-Hydroxysuccinimide (NHS) dilution were then added to activate the carboxyl groups of graphene oxide. Afterward, the obtained dilution was added into 50 mL of 4 mg L^{-1} chitosan solution and placed in ultrasonic for 15 min until it was dispersed in the chitosan solution. Subsequently, the beaker was placed in a 50ºC hot water bath for 3 h until the chitosan polymer had grafted on graphene oxide through an amide reaction between the carboxylic group of graphene oxide and the amine group of chitosan. Finally, the obtained adsorbent got separated from the solution utilizing a 1.4 Tesla magnet and then dried with a vacuum oven at 50ºC for 5 h (Fig.1).

6. Adsorption Experiments

300 mL of the Cu^{2+} dilution 2 mg L^{-1} was transmitted to a flask, and pH was regulated to 4.0 by adding 2 mL of the acetate buffer dilution. After that, 30 mg of the pre-synthesized adsorbent mGO-CS was added. Thereupon, to change the pH (4.0) of the dilutions, 2.0 mL of the buffer dilution (acetic acid/acetate 1.0 mol L^{-1}) was added. The resulted mix was blended on a shaker at 150 rpm for 25 min. After adsorption completion, the adsorbent got separated from the sample dilution using a 1.4 Tesla magnet. After that, 10 mL of 3 mol L^{-1} HNO_3 solution as a suitable eluent was added to the adsorbent and homogenized by a shaker for 5 min. Eventually, the adsorbent was separated again from the sample dilution using a 1.4 Tesla magnet. FAAS specified the Cu^{2+} concentration in the aqueous phase. For calculating the amount of metal ions removal by the adsorbent, the q_e (following equation) was utilized, where q_e is the number of metal ions adsorbed onto the unit amount of the adsorbent (mg g^{-1}), C_0 is the primary condensation of metal ions (mg L^{-1}), C_e represents the equilibrium amount of metal ions in the aqueous phase (mg L^{-1}), V is the volume of the metal ions dilutions (L), and m is the dry weight (g L^{-1}) of the adsorbent. The adsorption tests were done three times, and the mean values were offered.

$$q_e = \frac{(C_o - C_e)V}{m} \quad (1)$$

The removal effectiveness of each experimental ion was specified by the following equation, where R shows the removal effectiveness of each ion from the practical dilution, C_0 is the initial condensation, and C_e represents the final condensation after finishing the contact time with the adsorbent (mg L^{-1}).

$$\%R = \frac{(C_o - C_e)}{C_o} \times 100 \quad (2)$$

As shown in Fig. 2, mGO-CS possesses expressive improvements over GO and mGO to remove Cu^{2+} ions.

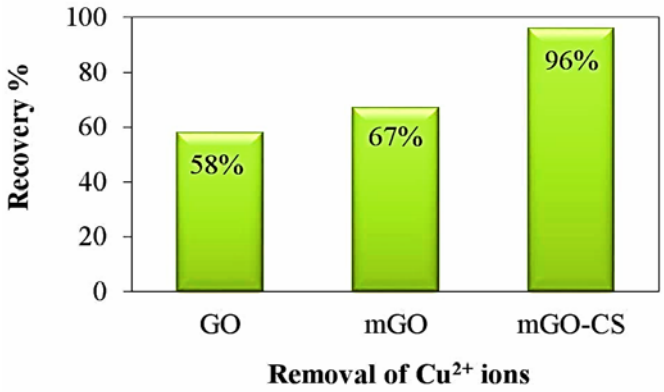

Fig. 2 – The trends of Cu^{2+} ions removal in different synthesis stages of adsorbent.

RESULTS AND DISCUSSION

1. Characterization of the Adsorbent

1.1. IR Spectra Analysis

Fig. 3(a) depicts the findings concerning the FT-IR spectrum. Based on GO, the spectra of 1055, 1207, 1401, 1629, 2923, and 3443 cm^{-1} revealed graphene oxide. In this figure, the 1055 cm^{-1} spectrum signifies the C–O bond. The peak observed at 1629 cm^{-1} is associated with the tensile C=O bond. The peak observed at 2923 cm^{-1} represents the symmetrical C–H tensile bond. The peak at 3443 cm^{-1} is related to the –OH stretching mode hydroxyl group on GO, which could be reported as the carboxyl group's variation. Further, the peak that emerged at 1401cm^{-1} is ascribed to C–OH stretching vibrations on graphene oxide. Epoxy and alkoxy functional groups are also located at around 1207 cm^{-1} and 1055 cm^{-1}, respectively.[12] In Fig. 3(a), mGO, which shows the magnetic graphene oxide, the peak at 695 cm^{-1}, is related to the Fe–O bond of Fe_3O_4 on synthesized adsorption.[13] Analyzing the IR spectrum according to Fig. 3(a) mGO-CS, in which the band is located at 1562 cm^{-1}, could indicate the successful amidation branched mGO sheets after adding chitosan and grafting of NH_2 groups onto the functional groups of mGO-CS. Furthermore, OH and NH_2 overlapped, making a broad peak in the range of 3457 cm^{-1}, related to the vibration of OH– and NH_2-chitosan chemical groups with oxygenated functional groups of graphene oxide (carboxylic and epoxy). The novel bands at 1479 and 1562cm^{-1} in the mGO-CS spectrum are associated with CH_2– and CONH–, respectively. Moreover, the bands at 1295 and 1132 cm^{-1} in mGO-CS sheets are attributed to the stretching of C–N and –NH_2 groups. Fig. 3(a) mGO-CS-Cu represents notable shifts in the intensity and location of peaks following the Cu^{2+} absorption procedure. The band shifting from 1642 cm^{-1} to 1649 cm^{-1} in the spectrum is described to the involvement of functional groups in the uptake of Cu^{2+}.[12,14]

1.2. XRD Analysis

In Fig. 3(b) GO, the diffraction created at 2θ=10.45º represents the graphene oxide. This issue is due to the oxidation of graphite sheets and their conversion to graphene oxide, while the diffraction produced at 2θ= 26.44º signifies graphite.[15] In Fig. 3(b) mGO, the diffraction of 2θ at 25.21º, 32.53º, 41.15º, 54.49º, 58.41º, and 66.02º on the planes of (220), (311), (400), (422), (511) and (440) degree, respectively, is associated with Fe_3O_4 nanoparticles. The XRD pattern also characterized the isometric crystal system for the synthesized sample. The entirely black color of the sample and its high magnetic power could shed light on the fact that the non-magnetic phases inside it are microscopic. Consequently, conducting experiments under the nitrogen atmosphere caused the particles to lack non-magnetic impurities, and therefore, it could be noted that magnetic graphene oxide was effectively synthesized.[16] Based on Fig. 3(b), mGO-CS, a weak and broad peak was witnessed at 2θ=27.31º, which could be attributed to the bond between the amine group in the chitosan and the carboxyl group in the graphene oxide. In Fig. 3(b) mGO-CS-Cu, the alteration in the intensity of 2θ and the slight shift in the peaks indicates the absorption of Cu^{2+} with the synthesized magnetic nano adsorbent, in which the intensity of 2θ decreased on the contrary to the previous stage, and the copper ions were removed.[17]

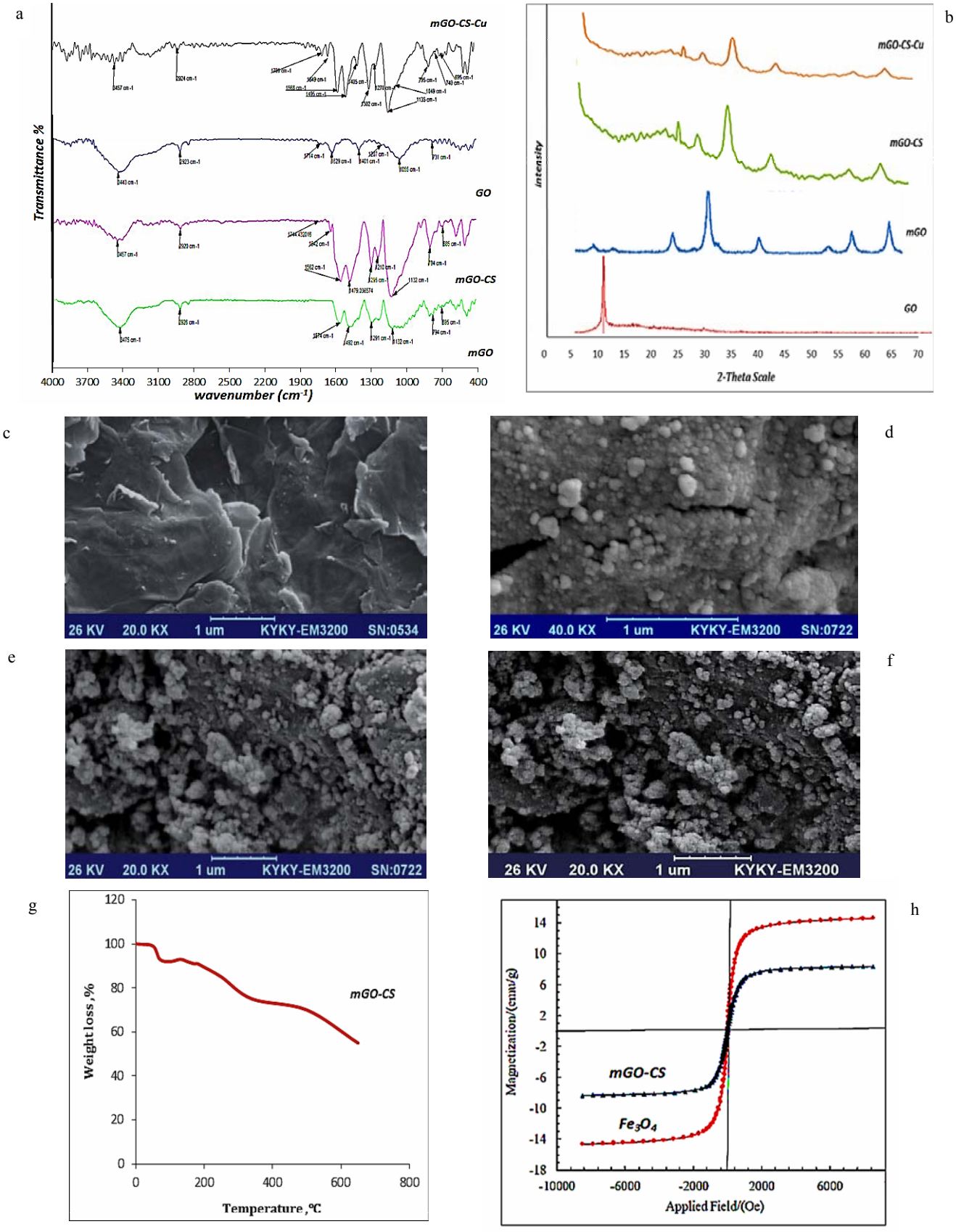

Fig. 3 – Characterization of the adsorbent: (a) FTIR pattern of GO, mGO, mGO-CS, mGO-CS-Cu; (b) XRD pattern of GO, mGO, mGO-CS, mGO-CS-Cu; (c) SEM image of GO; (d) SEM image of mGO; (e) SEM image of mGO-CS; (f) SEM image of mGO-CS-Cu; (g)TGA analysis of mGO-CS; (h) VSM magnetization curves of Fe_3O_4 and mGO-CS.

1.3. SEM Images

Fig. 3(C) indicates the typical SEM images of GO obtained employing a modified Hummers method. It offers a sheet-like structure with a wrinkled edge, a smooth surface, and large thickness. SEM spectrum in Fig. 3(d) displays that graphene oxide, which has a sheet form and proper porosity, was covered in its whole surface by iron oxide particles, polygonal and asymmetric. It indicated that they were magnetized, and the synthesized adsorbent had a moderately uniform porosity at the surface. This issue improved the contact surface of the contaminant with the adsorbent, thereby enhancing the adsorption efficacy. Fig. 3(e) demonstrates that the porous spaces on the adsorbent surface were occupied by chitosan, and graphene oxide dispersion was enhanced. In other words, the carboxylic acid in graphene oxide was bonded to the structure of the amine in chitosan, which revealed that the magnetic graphene oxide was functionalized with chitosan. It could be seen in Fig. 3(f) that with more luminous particles were absorbed on the adsorbent, their dispersion was more remarkable, and the clumping state decreased, confirming the adsorption of Cu^{2+} on the surface of the chitosan-functionalized magnetic graphene oxide.[18]

1.4. TGA Analysis

As shown in Fig. 3(g) mGO-CS, unlike pure graphene oxide, the magnetic nanocomposite of graphene oxide-chitosan showed three stages of weight loss. At this stage, the first weight loss happened at temperatures below 100ºC because of residual moisture evaporation in the nanocomposite. The second stage of weight loss took place in the temperature range of 160–200ºC, accounting for 10% of the total weight loss of nanocomposite. This is correlated with the weight loss of functional groups of graphene oxide, which happened at a lower temperature than its pure counterpart. Considering the pure graphene oxide in this temperature range, the reduced rate of nanocomposite weight loss indicated the formation of strong covalent bonds between graphene oxide and magnetic chitosan. The third weight-loss stage occurred at 470ºC, which is also associated with the degradation of chitosan.[19]

1.5. VSM Analysis

A Vibrating Sample Magnetometer (VSM) was utilized to examine the magnetic property of the nanocomposite. Fig. 3(h) plots the magnetic curve at room temperature for Fe_3O_4 magnetic particles at 15 emu g^{-1}. In contrast, the magnetic curve for magnetic nanoparticles of graphene oxide-chitosan (mGO-CS) at 8 emu g^{-1} is revealed in Fig. 3(h). The plot is based on the fact that chitosan and graphene oxide nanocomposite were magnetized with iron oxide particles and were thus easily absorbed by the magnet. As could be witnessed, the magnetic property reduced from 15 emu g^{-1} in iron oxide to 8 emu g^{-1}, which is because of the strong chemical bonds between the functional groups of graphene oxide and chitosan with iron oxide particles. Based on Fig. 3(h), it could be argued that the magnetic feature led the synthesized nanoparticles to be detached from the aqueous dilution by the magnet in a short time.[20]

2. Optimization of Adsorption Conditions

2.1. Effect of the pH

One of the essential parameters in studies on the extraction process and metal ion adsorption is the pH value of the sample solution. The present research evaluated the influence of pH on the quantity recovery of Cu^{2+} ions in a wide range of pH values (2–10). According to Fig. 4, the adsorption amount percentage and ion recovery of Cu^{2+} ions at pH=4 are maximum. The results indicate that the extraction efficiency decreased at the higher pH values (pH > 4). At lower pH (pH < 4), the removal process of Cu^{2+} ions could not be entirely performed due to the protonation of nitrogen groups in acidic media resulting in the decreased tendency to form the complex with Cu^{2+} ions. At alkaline media, hydroxide Cu^{2+} ions react to form $Cu(OH)_2$ precipitations. Therefore, the best complex formation constant between Cu^{2+} ion and chitosan amine group (NH_2) is established at pH=4.[21]

2.2. Effect of the amount of sorbent

The amount of adsorbent is the most influential parameter in quantity recovery and ion extraction processes. Various amounts of adsorbent within 5–150 mg L^{-1} were examined to estimate the optimum amount of adsorbent. According to Fig. 5, the optimum amount of adsorbent is 30 mg L^{-1}, where the adsorption percentage and recovery values for Cu^{2+} ions are maximum. Thus, it is evident that by introducing the new active adsorption sites, the ion removal process increases

while increasing surface availability positions for ion adsorption and enhancing the adsorption efficiencies. However, at lower adsorbent dosages, the accessible active sites for ions adsorption are rapidly saturated, leading to a noticeable reduction in adsorption efficiencies.[22]

2.3. Effect of contact time

The other important factor in the adsorption efficiency is the contact time between the adsorbent and the analyte in the sample solution. Hence, the recovery of Cu^{2+} ions at time intervals of 1–30 min was investigated. As seen in Fig. 6, absorption increases over time, and the quantity recovery of Cu^{2+} ions takes place at 25 min. In fact, after 25 min the equilibrium reaction between Cu^{2+} ions and adsorption occurs, and the adsorption process ends. At the initial process, due to empty accessible adsorption sites, the adsorption process rate is impressive. In contrast, after equilibrium time, the active surface contact sites get saturated, and the adsorption efficiency decreases.[23]

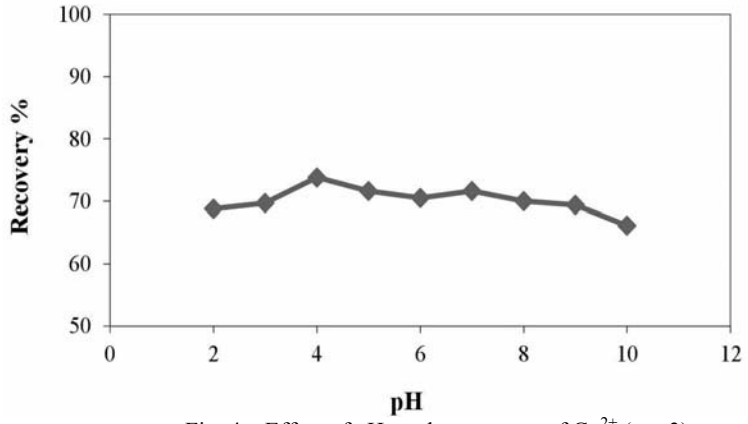

Fig. 4 – Effect of pH on the recovery of Cu^{2+} (n = 3).

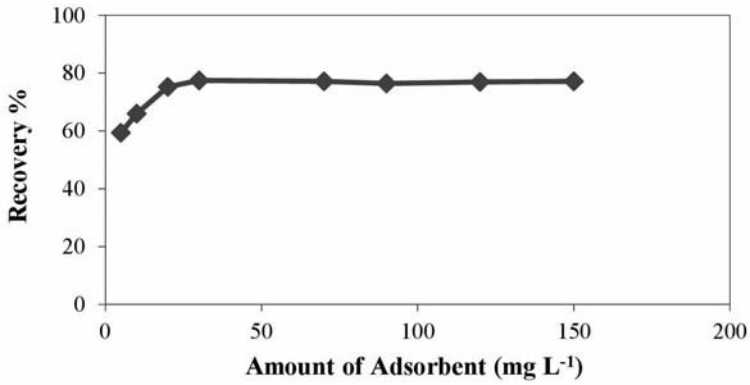

Fig. 5 – Effect of amount of adsorbent on the recovery of Cu^{2+} (n = 3).

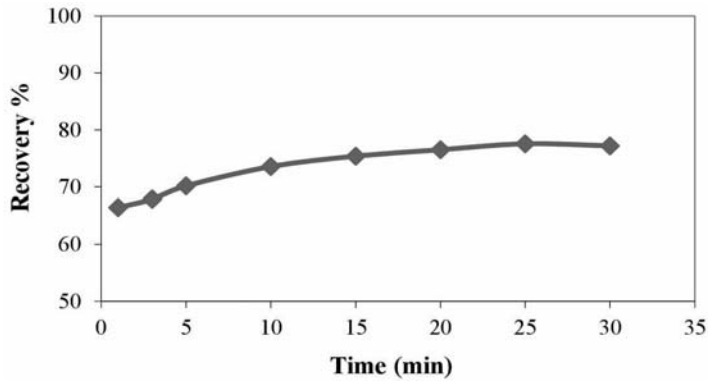

Fig. 6– Effect of time of adsorbent on the recovery of Cu^{2+} (n = 3).

2.4. Effect of eluent type

The eluent type also significantly increases the recovery and adsorption efficiencies, which should be selected carefully. According to the obtained results (Fig. 7), the recovery and leaching power of HNO_3 for Cu^{2+} ions is much higher than other acids. Acidic environments dissolve possible precipitation and increase recovery. Indeed, H^+ ions in a competitive practice are replaced by Cu^{2+} ions on the adsorbent surface and increase the extraction of these ions. Finally, 3 mol L^{-1} HNO_3 was considered as the appropriate eluent in the other adsorption processes.[24]

2.5. Effect of eluent volume

After finding the best eluent solvent, the impact of solvent volume on the adsorption process in the range of 5–20 mL was investigated. As shown in Fig. 8, 10 mL of 3 mol L^{-1} HNO_3 was selected as the optimum eluent solvent volume.[23]

2.6. Effect of sample volume

In this study, the impact of finding the appropriate sample volume on the recovery of Cu^{2+} ions in the range of 50–600 mL was evaluated. The findings in Fig. 9 show that up to 300 mL of Cu^{2+} ions solution, the Cu^{2+} ions are adsorbed on the adsorbent surface, the more Cu^{2+} ions will not be retained on the adsorbent. They will be removed from the adsorbent surface without inhibition.[25]

2.7. Effect of Foreign Ions

In each method, foreign ions are defined as ions causing about 5% error in the sample determination process. To evaluate the impact of foreign ions for the determination of Cu^{2+} ions by the proposed method, a specific concentration of foreign ions was added to initial Cu^{2+} ions solutions. The absorption of recovery Cu^{2+} ions solution with and without foreign ions was determined and compared. According to Table 1, the effect of foreign ions on Cu^{2+} ions concentration is no more than 5% error indicating that the foreign ions have no significant impact on the determination of Cu^{2+} ions concentration.[26-27]

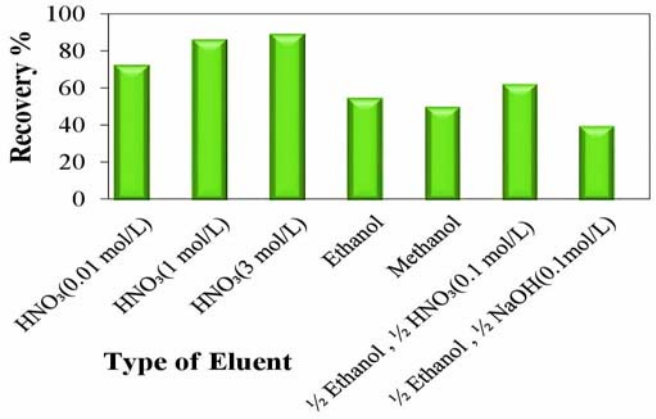

Fig. 7– Effect of eluent type on the recovery of Cu^{2+} (n = 3).

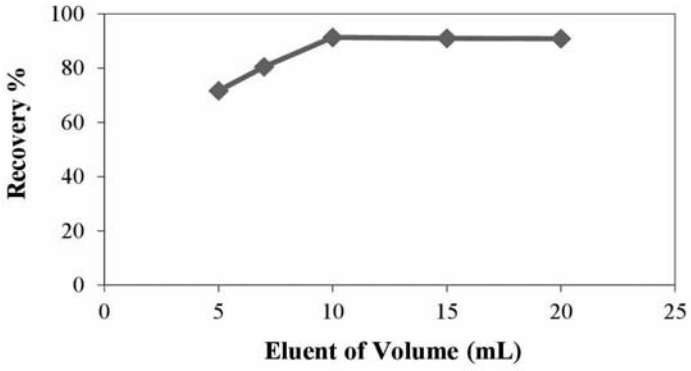

Fig. 8 – Effect of eluent volume on the recovery of Cu^{2+} (n = 3).

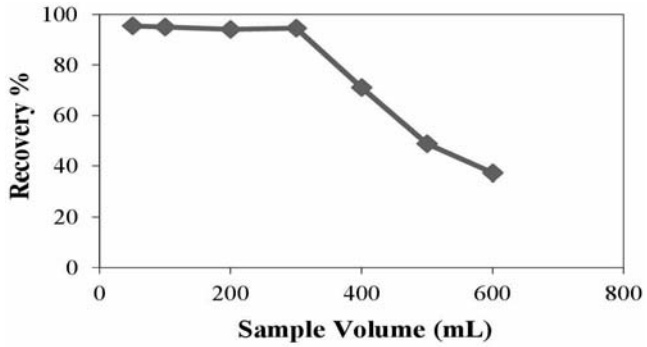

Fig. 9 – Effect of sample volume on the recovery of Cu^{2+} (n = 3).

Table 1

Effect of foreign ions on the percent recovery of ion Cu^{2+} in water samples (n = 3).

Diverse ion	Added as	Concentration (μg mL^{-1})	Recovery (%)
Na^+	NaCl	5000	98.18 ± 2.38 [a]
K^+	KCl	5000	92.33 ± 2.61
Mg^{2+}	$MgCl_2.6H_2O$	100	95.88 ± 1.03
Zn^{2+}	$Zn(NO_3)_2{\cdot}6H_2O$	5	97.54 ± 1.35
Ni^{2+}	$Ni(NO_3)_2$	5	93.72 ± 1.29
CO_3^{2-}	Na_2CO_3	1500	94.79 ± 0.93
Ag^+	$AgNO_3$	5	93.88 ± 1.28
SO_4^{2-}	Na_2SO_4	1500	96.29 ± 1.58
Cd^{2+}	$Cd(NO_3)_2{\cdot}4H_2O$	5	97.95 ± 1.63
Cl^-	KCl	5000	94.80 ± 2.04
Ca^{2+}	$CaCl_2.6H_2O$	1000	92.98 ± 1.17
Mn^{2+}	$Mn(NO_3)_2$	5	95.46 ± 1.81

a) Mean ± standard deviation.

3. Adsorption isotherms

Isotherm is the most critical parameter in designing the adsorption systems, which explains the association between adsorbent concentration and the adsorption capability of an adsorbent. In this study, Langmuir and Freundlich isotherm models were utilized. The Langmuir isotherm (Eq. 3) is based on the monolayer and uniform adsorption of adsorbent on all adsorbent surfaces. In contrast, the Freundlich isotherm (Eq. 4) is based on the multilayer and heterogeneous adsorption of adsorbent on the adsorbent.

$$\frac{C_e}{q_e} = \frac{1}{k_L q_{max}} + \frac{C_e}{q_{max}} \tag{3}$$

$$\ln q_e = \ln K_f + \frac{1}{n\,(\ln C_e)} \tag{4}$$

were q_e is the adsorbed number of the metal ion uptake with the adsorbent (mg g^{-1}), C_e is the condensation of metal ions at equilibrium (mg L^{-1}), K_L (L mg^{-1}) is the Langmuir adsorption equilibrium constant, q_{max} (mg g^{-1}) is the maximum adsorption capacity. K_F (mg g^{-1})(mg $L^{-1})^{-n}$ and n are the Freundlich isotherm constants, where K_F is associated with adsorption capability, and n is referred to as the adsorption force.[28-29]

4. Kinetic studies

The kinetic describes the rate of chemical reactions and the effective parameters on the chemical reaction rate. This section investigated the removal process of Cu^{2+} ions by quasi-first-order (Eq. 5) and quasi-second-order (Eq. 6) kinetic models.

$$\frac{1}{q_t} = \frac{k_1}{q_e t} + \frac{1}{q_e} \tag{5}$$

$$\frac{t}{q_t} = \frac{1}{k_2 q_e^2} + \frac{t}{q_e} \tag{6}$$

where q_t (mg g^{-1}) is the adsorbed number of metal ion on adsorbent at time t, k_1 is the pseudo-first-order rate constant for the kinetic model (min^{-1}), t is time (min), and q_e (mg g^{-1}) is the adsorbed number of metal ion onto the synthesized adsorbent at equilibrium, and k_2 is the pseudo-second-order rate constant of adsorption (g(mg min)$^{-1}$).[29]

Table 2

Langmuir and Freundlich model parameters for the Cu^{2+} ions adsorption onto mGO-CS

	Isotherm model					
	Langmuir			Freundlich		
Metal ion	q_{max} (mg g^{-1})	K_L (L mg^{-1})	R^2	n	K_F (mg g^{-1})(mg $L^{-1})^{-n}$	R^2
Cu^{2+}	158.73	0.0152	0.9394	1.61	4.91	0.9912

Table 3

Estimated adsorption kinetic parameters for the adsorption of Cu^{2+}on mGO-CS

	Pseudo-first-order model			Pseudo-second-order model		
Metal ion	q_e (mg g^{-1})	K_1 (min^{-1})	R^2	q_e (mg g^{-1})	K_2 (g $mg^{-1}min^{-1}$)	R^2
Cu^{2+}	15.67	0.3416	0.9747	16.18	0.1189	0.9983

Table 4

Thermodynamic parameter data for the adsorption of Cu^{2+} on mGO-CS

Metal ion	T(K)	K_d (L g^{-1})	ΔG^o (kJ mol^{-1})	ΔS^o (kJ mol^{-1} K^{-1})	ΔH^o (kJ mol^{-1})	R^2
Cu^{2+}	288	22.67	-6.90	0.10	22.75	0.9973
	298	28.61	-7.93			
	308	38.30	-8.96			
	318	51.19	-9.99			

Table 5

Determination of Cu^{2+} in real water samples (n = 3).

Samples	Spiked (μg mL^{-1})	Found (μg mL^{-1})	Relative recovery (%)
Tap water	0.0	N.D [a]	–
	5.0	4.91 ± 1.04 [b]	98.21 ± 1.36
	20.0	19.83 ± 1.23	99.15 ± 2.03
Well water	0.0	N.D	–
	5.0	4.73 ± 2.06	94.60 ± 1.83
	20.0	19.31 ± 1.13	96.55 ± 1.31
Sea water	0.0	N.D	–
	5.0	4.69 ± 2.04	93.80 ± 1.47
	20.0	19.08 ± 1.28	95.40 ± 1.02
Waste water	0.0	3.11 ± 2.42	–
	5.0	7.68 ± 1.23	91.40 ± 2.03
	20.0	21.06 ± 1.07	89.75 ± 1.92

a) Not Detected.
b) Mean ± standard deviation.

5. Adsorption thermodynamic

The thermodynamic parameters depend on the adsorption process. They are calculated using equations Eqs. 7, 8, and 9 or by plotting lnK versus 1/T.

$$\ln K_d = \frac{\Delta S^\circ}{R} - \frac{\Delta H^\circ}{RT} \quad (7)$$

$$\Delta G^\circ = - RT \ln K_d \quad (8)$$

$$\Delta G^\circ = \Delta H^\circ - T\Delta S^\circ \quad (9)$$

where, enthalpy change (ΔH°) in (kJ mol^{-1}), entropy change (ΔS°) in (kJ $mol^{-1}K^{-1}$), Gibbs free energy change (ΔG°) in (kJ mol^{-1}), K_d is the sorption equilibrium constant (L g^{-1}), T is the temperature in (K) and R is the universal gas constant (8.314 J mol^{-1} K^{-1}).[16,30]

Table 6

Comparison of the suggested method with other studies

Method	Adsorbent	pH	PF	LOD(μg mL^{-1})	LOQ(μg mL^{-1})	R^2	RSD%	samples	Ref.
GA–DLPME–UV–Vis	–	6	122	0.07	0.23	0.9950	3.9	water samples	[31]
SPE–FAAS	MWCNTs	5	25	0.05	–	0.9991	< 10	water samples	[32]
Colorimetric–UV–Vis	L–cys–AgNPl	–	–	0.22	–	0.9991	< 8.46	water samples	[33]
MSPE–FAAS	mGO–CS	4	30	0.01	0.03	0.9971	2.16	water samples	This work

6. Determination of Cu^{2+} in Real Water Samples

To investigate the applicability of the suggested method and determine Cu^{2+} ions in actual samples, the concentration of Cu^{2+} ions was determined in several different aqueous and biological samples. These samples contain the following materials: Well water (Varamin, 18 January 2020), Tap water (taken after 10 min operation of the tap, Tehran, 22 January 2020), Sea water (taken from the Caspian Sea, 26 January 2020), and Waste water (taken from the Industrial effluent of Iran Khodro town, 2 February 2020). First, the sample was tested without adding a certain amount of Cu^{2+} ions. According to the supposed method, a certain amount of Cu^{2+} ions was added in the second step, and preconcentration and separation processes were performed. The results of this analysis are summarized in Table 5.

7. Comparison

According to Table 6, the proposed method is effective compared to the other methods since the adsorbent synthesized in this method is environmentally friendly and has a very high specific surface area for adsorption. The extraction rate in the MSPE method is high, and a magnet easily separates the synthesized adsorbent due to its magnetic properties. Furthermore, the other benefits of the suggested method are its rapid extraction rate, low detection limit, availability, and higher efficiency.

CONCLUSION

This study used the synthesized magnetic nanocomposite (mGO-CS) as an effective adsorbent with high efficiency to remove Cu^{2+} ions from various aqueous solutions using magnetic solid-phase extraction (MSPE). All impressive parameters influencing the extraction process were investigated and optimized. The isothermal data of equilibrium adsorption are in agreement with the Freundlich isotherm model. The kinetic studies of the removal process reveal that the removal process of Cu^{2+} ions follows the pseudo-second-order kinetic model. The obtained thermodynamic data of the removal process indicated that the removal process of Cu^{2+} ions is endothermic ($\Delta H > 0$) and spontaneous ($\Delta G < 0$) in nature. In addition, it is accompanied by an increase in entropy ($\Delta S > 0$), indicating the disordering of Cu^{2+} ion increases during the adsorption process. Finally, the suggested method provides an efficient technique with significant properties such as high sensitivity, good repeatability, rapid separation rate, high adsorption capability, good recovery, and low detection limit to determine a trace amount value of Cu^{2+} ions in different aqueous samples.

REFERENCES

1. A. Moghimi, M. Abniki, M. Khalaj and M. Qomi, *Rev. Roum. Chim.,*, **2021**, *66*, 493-507.
2. A. Moghimi and M. Abniki, *Adv. J. Chem.-Section A*, **2021**, *4*, 78-86.
3. M. Abniki, A. Moghimi and F. Azizinejad, *J. Chin. Chem. Soc.*, **2021**, *68*, 343-352.
4. F. Sharifianjazi, A. Jafari Rad, A. Bakhtiari, F. Niazvand, A. Esmaeilkhanian, L. Bazli, M. Abniki, M. Irani and A. Moghanian, *Biomed. Mater.*, **2021**, *17*, 012002.
5. A. Moghimi and M. Abniki, *J. Color Sci. Techn.*, **2022**, *15*, 301-315.
6. T. Pourshamsi, F. Amri and M. Abniki, *J. Iran. Chem. Soc.*, **2021**, *18*, 245-264.
7. A. Moghimi and M. Abniki, *Russ. J. Phys. Chem. B*, **2021**, *15*, S130-S139.
8. F. Einollahi Peer, N. Bahramifar and H. Younesi, *J. Taiwan Inst. Chem. Eng.,* **2018**, *87*, 225-240.
9. S. K. Yong, N. Bolan, E. Lombi and W. Skinner, *Water, Air, Soil Pollut.,* **2013**, *224*, 1720.

10. A. Kazemi, N. Bahramifar, A. Heydari and S. I. Olsen, *J. Cleaner Prod.,* **2018**, *174*, 527-537.
11. A. Sharif, M. Khorasani and F. Shemirani, *J. Inorg. Organomet. Polym. Mater.,* **2018**, *28*, 2375-2387.
12. W. Sun, L. Li, C. Luo and L. Fan, *Int. J. Biol. Macromol.,* **2016**, *85*, 246-251.
13. F. Bianchi, V. Chiesi, F. Casoli, P. Luches, L. Nasi, M. Careri and A. Mangia, *J. Chromatogr. A,* **2012**, *1231*, 8-15.
14. M. Abniki, A. Moghimi and F. Azizinejad, *J. Serb. Chem. Soc.*, **2020**, *85*, 1223-1235.
15. G. Zhao, X. Ren, X. Gao, X. Tan, J. Li, C. Chen, Y. Huang and X. Wang, *Dalton Trans.,***2011**, *40*, 10945-10952.
16. R. Masoudi, H. Moghimi, E. Azin and R. A. Taheri, *Artif. Cells, Nanomed., Biotechnol.,* **2018**, *46*, S1092-S1101.
17. O. Arjmand, M. Ardjmand, A. M. Amani and M. H. Eikani, *BioNanoScience,* **2020**, *10*, 705-713.
18. K. Molaei, H. Bagheri, A. A. Asgharinezhad, H. Ebrahimzadeh and M. Shamsipur, *Talanta,* **2017**, *167*, 607-616.
19. Z. Lu, J. Yu, H. Zeng and Q. Liu, *Sep. Purif. Technol.,* **2017**, *183*, 249-257.
20. J.-H. Deng, X.-R. Zhang, G.-M. Zeng, J.-L. Gong, Q.-Y. Niu and J. Liang, *Chem. Eng. J.,* **2013**, *226*, 189-200.
21. Y. Cui, S. Liu, Z.-J. Hu, X.-H. Liu and H.-W. Gao, *Microchim. Acta,* **2011**, *174*, 107.
22. S. P. Dubey and K. Gopal, *J. Hazard. Mater.,* **2007**, *145*, 465-470.
23. M. Abniki, Z. Azizi and H. A. Panahi, *IET nanobiotechnology*, **2021**, *15*, 664-673.
24. Z. Erbas, M. Soylak, S. Ozdemir and E. Kilinc, *Int. J. Environ. Anal. Chem.,* **2019**, *99*, 1112-1122.
25. A. Moghimi, M. Qomi, M. Yari and M. Abniki, *Int. J. Bio-Inorg. Hybr. Nanomater*, **2019**, *8*, 163-172.
26. A. Moghimi, *Russ. J. Phys. Chem. A,* **2013**, *87*, 1203-1209.
27. G. S. Kanberoglu, E. Yilmaz and M. Soylak, *J. Iran. Chem. Soc.,* **2018**, *15*, 2307-2314.
28. M. Abniki, A. Moghimi, *Micro Nano Lett.*, **2021**, *16*, 455-462.
29. A. Moghimi and M. Abniki, *Chem. Method.*, **2021**, *5*, 250-258.
30. R. Motallebi, A. Moghimi, H. Shahbazi and H. Faraji, *Rev. Roum. Chim*., **2020**, *65*, 293-305.
31. M. Akhond, G. Absalan, T. Pourshamsi and A. M. Ramezani, *Talanta,* **2016**, *154*, 461-466.
32. S. Vellaichamy and K. Palanivelu, *J. Hazard. Mater.,* **2011**, *185*, 1131-1139.
33. N. Poosinuntakul, T. Parnklang, T. Sitiwed, S. Chaiyo, S. Kladsomboon, O. Chailapakul and A. Apilux, *Microchem. J.,* **2020**, *158*, 105101.